Effects of Immediate and Delayed Loading on Peri-Implant Trabecular Structures: A Cone Beam CT Evaluation

Yan Huang, DDS;[*,†] Jeroen Van Dessel, MSc;[*] Xin Liang, DDS, PhD;[‡] Maarten Depypere, MSc;[§] Weijian Zhong, DDS;[‡] Guowu Ma, DDS, PhD;[‡] Ivo Lambrichts, DDS, PhD;[¶] Frederik Maes, PhD;[§] Reinhilde Jacobs, DDS, PhD[*]

ABSTRACT

Purpose: To develop a method for characterizing trabecular bone microarchitecture using cone beam computed tomography (CBCT) and to evaluate trabecular bone changes after rehabilitation using immediate versus delayed implant protocols.

Materials and Methods: Six mongrel dogs randomly received 27 titanium implants in the maxillary incisor or mandibular premolar areas, following one of four protocols: (1) normal extraction socket healing; (2) immediate implant placement and immediate loading; (3) delayed implant placement and delayed loading; (4) delayed implant placement and immediate loading. The animals were euthanized at 8 weeks, and block biopsies were scanned using high resolution CBCT. Standard bone structural variables were assessed in coronal, middle, and apical levels.

Results: Coronal and middle regions had more compact, more platelike, and thicker trabeculae. Protocols (2), (3), and (4) had significantly higher values ($p < 0.001$) than protocol (1) for bone surface density, bone surface volume ratio, and connectivity density, while significantly lower values ($p < 0.001$) were found for trabecular separation and fractal dimension. However, protocols (2), (3), and (4) did not show significantly different bone remodeling.

Conclusions: Compared with normal extraction healing, the implant protocols have an improved bone structural integration. Results do not suggest a different bone remodeling pattern when a delayed versus an immediate implant protocol is used.

KEY WORDS: animal experiments, cone beam CT, dental implants, immediate loading, trabecular bone

INTRODUCTION

While traditional dental implant protocols incorporate a healing period prior to placing the implant (delayed implant placement), several attempts have been reported and specific treatment protocols introduced in order to reduce the total treatment time. The advent of new implant materials, surface coating, and adaptations to the mechanical design has opened up the path toward immediate implant placement, thus increasing patient comfort by shortening treatment periods, while preserving some of the bone volume.[1] Some clinical studies found similar implant survival rates and marginal bone loss in the short and medium term when comparing delayed and immediate implant placement protocols.[2,3] Moreover, several histological studies on humans and experimental animals suggested that immediate loading implants show a higher percentage of bone-to-implant contact (BIC) than either delayed loading implants or implants left unloaded.[4–6] Nevertheless, the available

[*]Oral Imaging Center, Department of Oral Health Science, KU Leuven, Leuven, Belgium; [†]Oral Implant Center, West China College of Stomatology, Sichuan University, Chengdu, China; [‡]School of Stomatology, Dalian Medical University, Dalian, China; [§]ESAT/PSI, Medical Image Computing, KU Leuven, Leuven, Belgium; [¶]Laboratory of Histology, Biomedical Research Institute, Hasselt University, Diepenbeek, Belgium

Reprint requests: Professor Xin Liang, School of Stomatology, Dalian Medical University, Dalian 116044, China; e-mail: lilyliang13@hotmail.com

DOI 10.1111/cid.12063

literature has so far not conclusively determined the superiority of immediate loading protocols, particularly with regard to the three-dimensional microstructure of peri-implant bone.

The survival rate of implants is significantly affected by bone quality,[7] which not only relates to bone mineral density but also critically depends on the three-dimensional microstructure of the peri-implant bone.[8] Trabecular bone is more metabolically active than cortical bone[8] and therefore is a more sensitive indicator of early physiopathologic changes. Consequently, objective quantitative assessment of trabecular architecture around the implant may provide comprehensive structural information related to different implant placements for better determining the status of osseointegration.

For decades, the most common method used to evaluate peri-implant tissue has been histomorphometry, which allows two-dimensional measurements on thin histological sections. As this classical technique is invasive, time-consuming, and prone to sampling errors, three-dimensional imaging using microcomputed tomography (μCT) has been validated as a non-invasive and accurate method for assessment of bone geometry.[9] Yet although μCT has been widely applied for three-dimensional evaluation of trabecular structures in bone biopsies and small animal bones,[9,10] it is of limited use at present in the clinical routine. For imaging of trabecular bone in vivo, both high-resolution magnetic resonance imaging (HR-MRI) and multidetector CT (MDCT) have been investigated.[11,12] However, the potential of MRI is limited by the long scan times needed to obtain high-resolution imaging of trabecular bone and by metal artifacts because of magnetic susceptibility.[13] MDCT, on the other hand, requires substantial radiation exposure to achieve enough spatial resolution.[14] Recently, low-dose dental cone beam CT (CBCT) has become widely available in clinical practice as a new technique for rapid non-invasive imaging at even higher image quality than MDCT.[14] Whereas the accuracy of CBCT in the measurement of bone-related parameters (e.g., bone thickness) has been investigated thoroughly,[15] little is known about the potential of CBCT for analyzing peri-implant trabecular bone morphology.

Therefore, the purpose of the present study was to evaluate the three-dimensional morphology of peri-implant trabecular bone in a dog model after 2 months of immediate and delayed implant protocols, by means of high-resolution CBCT.

MATERIALS AND METHODS

The experimental protocol was approved by the bioethics committees of Dalian Medical University, Hasselt University, and KU Leuven (P059-2012-TK). A split-mouth randomized design, using four treatment protocols on six tooth positions in six male mongrel dogs (Table 1), was employed. The dogs (weight 14.8–18.1 kg, age 20–24 months old) were without any oral or systemic diseases and were housed individually in indoor cages. The diet during the course of the experiment was whole grain flour, cornmeal, soybean cake, fishbone meal, and eggs according to the general feeding program at the Experimental Animal Center of Dalian Medical University, China. The whole surgical procedure was

TABLE 1 Random Distribution of Split-Mouth Design in Six Experimental Dogs

Dog	I (R)	I (L)	P3 (R)	P3 (L)	P4 (R)	P4 (L)
1	Control	DIP + DL	DIP + DL	DIP + IL	Control	IIP + IL
2	DIP + DL	DIP + IL	DIP + IL	IIP + IL	DIP + DL	Control
3	DIP + IL	IIP + IL	IIP + IL	Control	DIP + IL	DIP + DL
4	IIP + IL	Control	Control	DIP + DL	IIP + IL	DIP + IL
5	Control	DIP + DL	DIP + DL	DIP + IL	Control	IIP + IL
6	DIP + DL	DIP + IL	DIP + IL	IIP + IL	DIP + DL	Control

In total, 36 samples were used in the study (Control = 9; IIP + IL = 8; DIP + DL = 10; DIP + IL = 9). The investigators ensured unpredictability of the allocation sequence by coin toss before surgeries.

I, 3rd maxillary incisors; P3, 3rd mandibular premolars; P4, 4th mandibular premolars; R, right side; L, left side; DIP, delayed implant placement; IIP, immediate implant placement; DL, delayed loading; IL, immediate loading.

performed by one and the same surgeon (W.Z.), with a decade of clinical experience in implant dentistry. The surgeon was blinded to the allocation process, but once tooth extraction had been carried out, he could no longer be blinded to the allocated implant placement.

Surgical Procedures

Tooth Extraction. The dogs got 1 week of antibiotics prophylaxis (gentamicin sulfate, 1 600 000 U/day, Lingrui Pharmaceutical Co. Ltd, Zhengzhou, China) to prevent infection. In each dog, bilateral 3rd and 4th mandibular premolars (P3 and P4) as well as 3rd maxillary incisors (I) were chosen as the implant recipient sites (Figure 1A). During all surgical procedures, the dogs were anesthetized with Sumianxin (0.1 ml/kg xylazine hydrochloride, Changchun Military Academy of Medical Sciences, Changchun, China). Local anesthesia (2–4 ml lidocaine 2% with epinephrine 1:100 000, Tianjin Pharmaceutical Co. Ltd, Tianjin, China) was used at the surgical site. After tooth extraction, these sites were sutured with 4-0 vicryl resorbable sutures.

Implant Placement. Sample size calculation was based on a preliminary experiment. Given $\alpha = 0.05$ and $\beta = 0.10$, it was calculated that at least seven samples in each group were needed to reach significance level for connectivity density (Conn.dn) when differences of 3.5 mm^{-3} and a standard deviation of 2 mm^{-3} were assumed. Twenty-seven custom-made threaded implants of grade 5 pure titanium (machined surface, Ø = 3.1 mm for I and 4.1 mm for P3 and P4, L = 11 mm, Figure 1B) were thoroughly examined first to reject failed test pieces and were sterilized prior to surgery. Each implant recipient site was randomly assigned to one of four treatment protocols (Figure 2), and two-stage implant placement was applied accordingly: (1) control group ($n = 9$); (2) immediate implant placement and immediate loading group (IIP + IL, $n = 8$); (3) delayed implant placement and delayed loading group (DIP + DL, $n = 10$); (4) delayed implant placement and immediate loading group (DIP + IL, $n = 9$).

Before insertion, to ensure that the shoulder of the implant was placed at the level of the marginal bone, each site was drilled at low speeds (800 rpm) while being cooled with sterile saline at 4°C. Implants were placed under the same surgical conditions as the tooth extractions in terms of sterility, operation room, and anesthesia. The primary stability of implants was checked after implant insertion by percussion testing, which was carried out by making a simple percussion with the

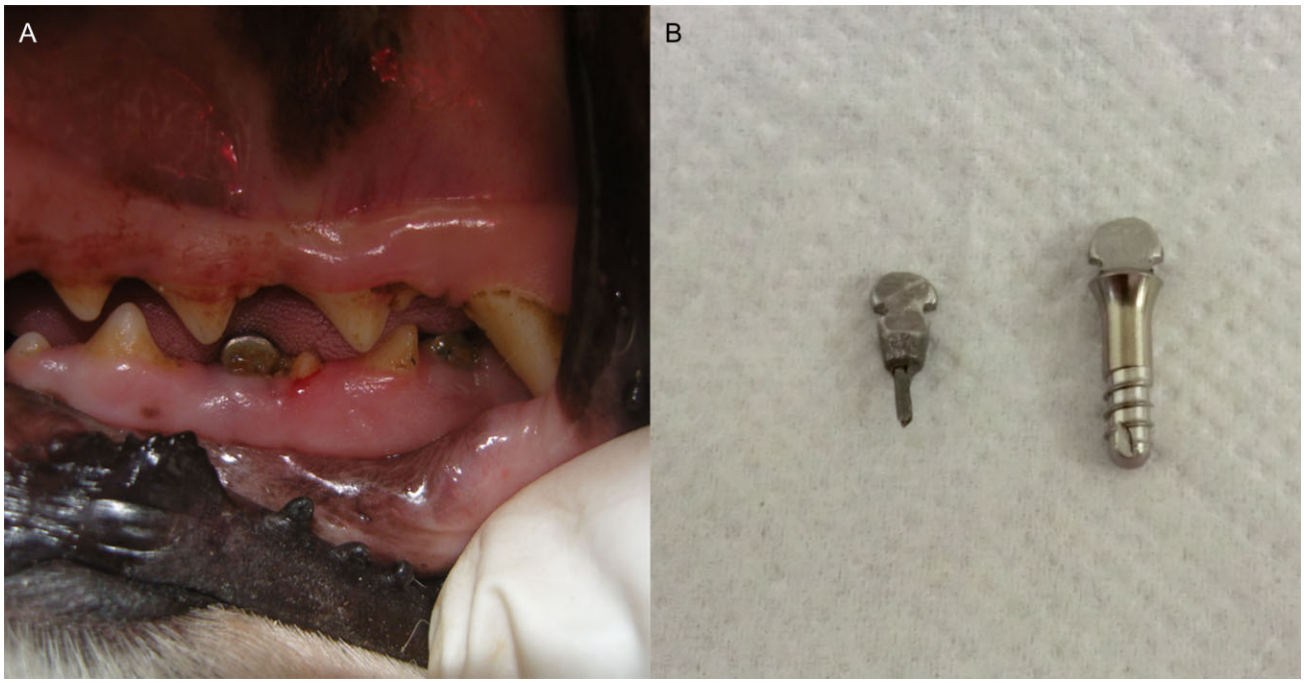

Figure 1 Implant recipient sites and the custom-made implant, post, and crown used in the study. (A) Mesial part of P3 and distal part of P4 were extracted, while the distal part of P3 and mesial part of P4 were kept in the socket. (B) Custom-made titanium implant and NiTi-based post and crown.

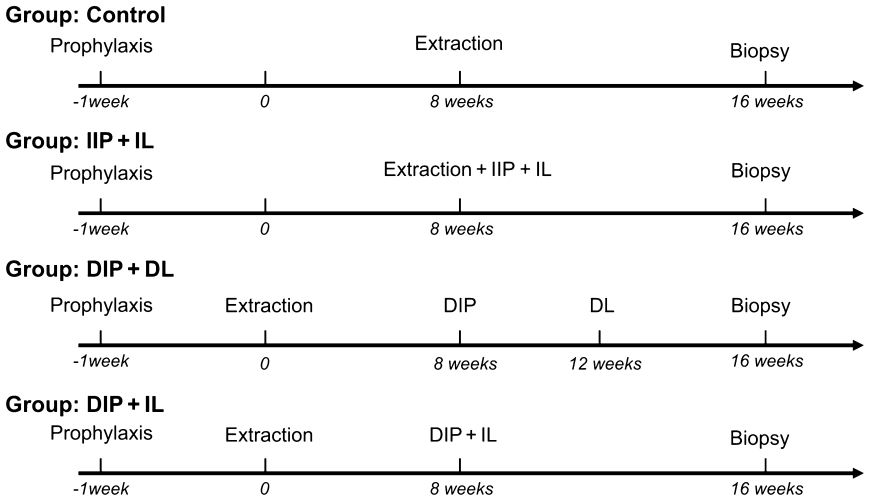

Figure 2 Time frame for different protocols. DIP = delayed implant placement; DL = delayed loading; IIP = immediate implant placement; IL = immediate loading.

handle of a dental instrument on the implant abutment while listening to the resulting sound to detect non-osseointegration. Then, customized posts with a crown made of NiTi alloy (College of Stomatology, Dalian Medical University, Figure 1B) were set using resin cement (RelyX, Unicem, RX, 3M ESPE, St. Paul, MN, USA). During the experimental period, the loading pressure on the implants was kept similar using 20-μm articulating papers (Accufilm II, RX, 3M ESPE). Combined with general anesthesia, plaque control was ensured three times per week using a 0.2% chlorhexidine gel on implant placement sites with a soft toothbrush.

Biopsies. At week 17 (Figure 2), all dogs were sacrificed by means of an intravenous injection of an overdose of Sumianxin and immediately perfused through the carotid arteries with a fixative solution of 4% paraformaldehyde and 0.0125% glutaraldehyde in 0.1 M phosphate buffer, pH 7.4. The jawbones were dissected and defleshed. Then, each implant was removed with a carefully preserved 3- to 5-mm piece of peri-implant bone as one piece of sample. The samples were placed into a sealable container with the fixative Unifix® (4% formaldehyde, Tianjin Chemical Reagent Company, Tianjin, China) for 3 weeks at 4°C.

Morphometric CBCT Analysis

Thirty-six samples were scanned using a high-resolution CBCT (3D Accuitomo 170, Morita, Tokyo, Japan), which had been calibrated before the radiographic study by the manufacturer at the time of installation and when updates were performed. Each sample was placed vertically in a sponge block in order to prevent any movement during the scanning process, with the long axis of the implant perpendicular to the scanning beam. All samples were scanned using the following exposure conditions: 0.08 mm voxel size, 360° rotation, 90 kV tube voltage, 2 mA tube current, 30.8-second scanning time, and a field of view (FOV) of 40×40 mm. Four ring-shaped volumes of interest (VOIs) were defined around the surface of the implant at coronal (A), middle (B), and apical (C1 and C2) sections along the axis of the implant, as indicated in Figure 3. The VOIs comprised trabecular bone only, which was selected through intermediate cross sections by using custom processing in the CTAn V1.11 (CTAnalyser, Skyscan, Antwerp, Belgium) (Figure 4). The irregular anatomic regions of interest (ROIs) were drawn in each section,[16] either manually in the case of the control group or automatically in the case of the implant protocols group, such that cortical bone in the ring-shaped ROIs was excluded, and only trabecular structures were retained for assessment.

Standard three-dimensional structural parameters of trabecular bone architecture (Table 2) were quantified from the CBCT images using CTAn on the VOIs, following the recommendations of the American Society of Bone and Mineral Metabolism[16] and Parfitt's system.[17] The examiner responsible for morphological analyses (J.V.D.) was blinded to the group allocation.

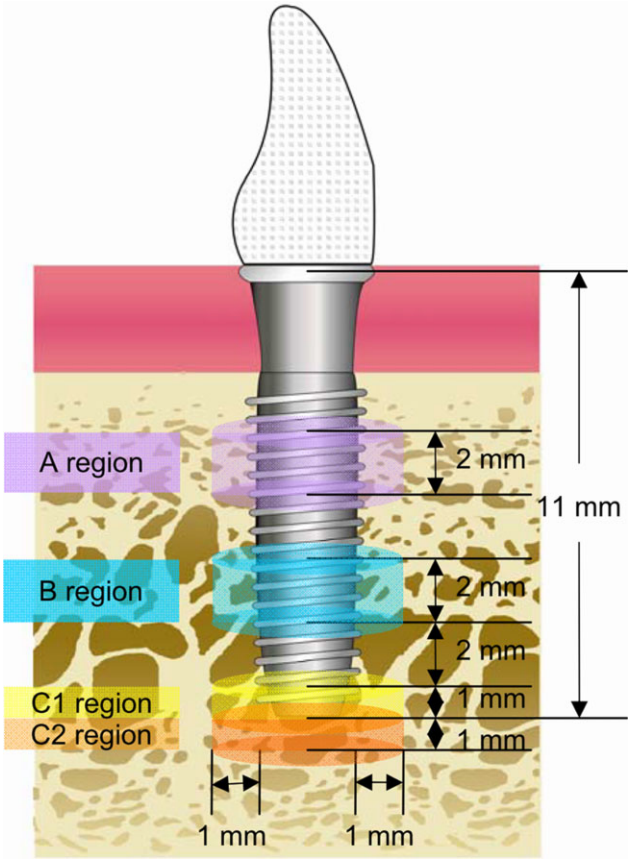

Figure 3 Schematic representation of the volumes of interest (VOIs) selected for regional morphometric analysis of peri-implant bone. Four different VOIs were defined in coronal (A), middle (B), and apical (C1 and C2) sections along the axis of the implant (width = 1 mm; height = 2 mm for A and B, 1 mm for C1 and C2).

Statistical Analysis

Descriptive analysis expressed data as central tendency and dispersion measurements. Fisher's exact test was used to compare variance between groups, followed by post hoc Tukey's HSD test, allowing multiple comparisons. Nonparametric statistical methods were used when normality was not confirmed. For all tests performed, the significance level α was 5%. Statistical analysis was performed in R 2.14.2 (R Development Core Team).

RESULTS

All animals recovered well after the surgery without any clinical signs of infection or inflammation, and all behaved normally throughout the experimental period. The surgical procedures and follow-up showed no complications regarding the procedural conditions, and all implants were clinically stable until euthanasia. Although trabeculae were clearly visible, they were not, overall, well defined. No artifacts were present in the CBCT images except that along the bone-implant direct interface, a thin blurred layer occurred due to titanium scatter, which was later reduced by custom-made CTAn software.

Three-Dimensional Morphometric Comparison of the Anatomical Regions

Morphometric parameters for the VOIs are summarized in Table 3. A one-sample Shapiro-Wilk test showed that most of the parameters were not normally distributed, except for bone volume fraction (BV/TV) and bone pattern factor (Tb.Pf). In the A, B, C1, and C2 regions, the same trend of central tendency and dispersion was visible.

The coronal and middle regions had higher BV/TV, specific bone surface (BS/BV), and Conn.dn values than the apical regions. Lower values for trabecular thickness (Tb.Th) and trabecular number (Tb.N) were found in the most apical region. However, the differences in these values between the coronal and apical trabeculae were not as large as for BV/TV, BS/BV, and Conn.dn. The apical trabecular bone exhibited much larger Tb.Pf and total porosity percentage (Po (tot)) compared with the coronal bone. The highest structural model index (SMI) values were found in the apical trabecular bone, which is characterized by rods (ideal rods: SMI = 3), and the lowest values were identified in the coronal and middle regions, showing more platelike structures (ideal plates: SMI = 0).

Three-Dimensional Morphometric Comparison of the Implant Protocols

Data from different anatomical regions were combined and were then compared according to different implant protocols. Statistical analyses revealed significant differences ($p < 0.001$) in bone characteristics for control versus IIP + IL, DIP + IL, and DIP + DL, and for BS/BV, fractal dimension (FD), trabecular separation (Tb.Sp), and Conn.dn (Table 4).

All implant protocols had significantly higher values than the control for BS/BV and Conn.dn, while significantly lower values were found for Tb.Sp and FD. However, no significant difference was observed between any two of the treatment groups. The highest values for BV/TV, Tb.N, and Conn.dn, as well as the

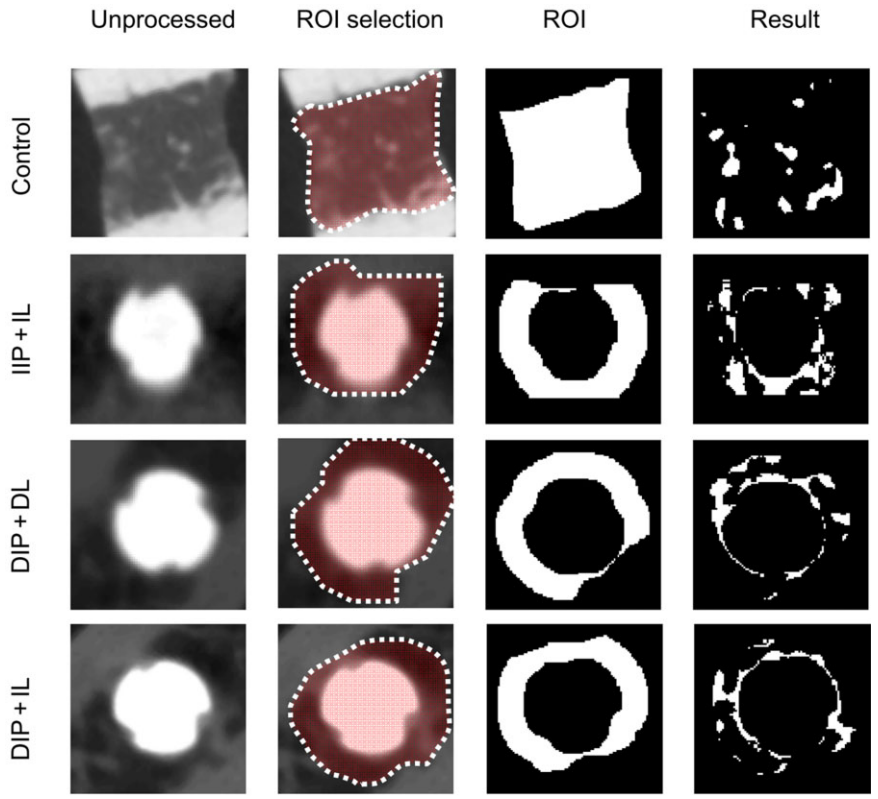

Figure 4 Quantification of regional bone morphometry from CBCT images for different implant protocols. From left to right: original CBCT image; manually rough selection of the region of interest (ROI) for the control (approximately 5 × 5 mm) and for the implant protocols; binary ROI automatically generated by a custom processing algorithm based on thresholding segmentation for the implant protocols, according to the specifications in Figure 3, excluding implant and cortical bone; binary segmentation of trabecular bone in this ROI, from which trabecular morphometric parameters were calculated. DIP = delayed implant placement; DL = delayed loading; IIP = immediate implant placement; IL = immediate loading.

TABLE 2 Parameters Quantified from CBCT Images for Regional Bone Morphometric Evaluation in Selected Volumes of Interest (VOIs)

Abbreviation	Morphologic Parameter	Standard Unit	Description
TV	Total volume of interest	(mm^3)	Volume of the entire region of interest
BV	Bone volume	(mm^3)	Volume of the region segmented as bone
BV/TV	Bone volume fraction	(%)	Ratio of the segmented bone volume to the total volume of the region of interest
BS	Bone surface	(mm^2)	Surface of the region segmented as bone
BS/BV	Specific bone surface	(mm^2/mm^3)	Ratio of the segmented bone surface to the segmented bone volume
Tb.Th	Trabecular thickness	(mm)	Mean thickness of trabeculae, assessed using direct three-dimensional methods
Tb.Sp	Trabecular separation	(mm)	Mean distance between trabeculae, assessed using three-dimensional methods
Tb.N	Trabecular number	(1/mm)	Measure of the average number of trabeculae per unit of length
Tb.Pf	Bone pattern factor	(1/mm)	Index of connectivity of bone
SMI	Structural model index		An indicator for the structure of trabeculae
FD	Fractal dimension		Measure of surface complexity of a trabecula
Po (tot)	Total porosity percentage	(%)	Ratio of the volume of all open plus closed pores to the total volume of interest
Conn.dn	Connectivity density	($1/mm^3$)	Measure of the degree of connectivity of trabeculae normalized by TV

TABLE 3 Descriptive Statistics of Three-Dimensional Morphometric Parameters for Different Anatomical Regions

Morphometric Parameters (unit)	Mean (SD)				Min-Max				Median			
	A	B	C1	C2	A	B	C1	C2	A	B	C1	C2
TV (mm^3)	33.34 (23.19)	39.98 (27.94)	21.48 (25.11)	21.21 (19.02)	12.11–114.90	12.70–93.21	5.98–113.47	9.42–66.14	23.98	24.91	10.15	10.80
BV (mm^3)	15.12 (10.63)	16.21 (10.57)	5.78 (5.92)	5.17 (5.50)	2.19–44.14	3.77–40.15	0.64–21.89	0.52–19.50	10.43	12.28	5.92	3.35
BV/TV (%)	44.59 (11.47)	43.88 (10.11)	28.73 (11.45)	24.49 (13.35)	15.37–71.63	24.67–62.32	8.14–52.58	4.77–46.05	43.65	44.49	31.00	24.11
BS (mm^2)	143.08 (72.76)	155.53 (79.31)	68.47 (59.68)	55.27 (54.46)	34.58–345.29	53.89–357.94	12.89–257.31	7.88–193.62	113.33	128.32	46.24	39.83
BS/BV (mm^2/mm^3)	10.75 (2.33)	10.55 (2.00)	14.27 (4.02)	11.77 (2.42)	5.01–15.76	5.50–14.63	9.31–26.51	8.14–17.01	10.74	10.38	13.32	11.17
Tb.Th (mm)	0.45 (0.06)	0.45 (0.05)	0.37 (0.07)	0.39 (0.08)	0.36–0.69	0.36–0.67	0.18–0.48	0.23–0.52	0.45	0.45	0.39	0.42
Tb.Sp (mm)	0.57 (0.15)	0.63 (0.21)	0.62 (0.15)	0.80 (0.19)	0.40–1.08	0.40–1.15	0.43–0.95	0.51–1.05	0.53	0.55	0.57	0.82
Tb.N (1/mm)	0.97 (0.19)	0.97 (0.19)	0.77 (0.25)	0.62 (0.30)	0.43–1.32	0.62–1.28	0.33–1.36	0.19–1.02	0.98	0.99	0.80	0.63
Tb.Pf (1/mm)	0.42 (1.65)	0.53 (1.17)	3.69 (1.86)	3.39 (2.16)	−3.44–3.77	−2.16–2.67	−0.33–8.01	−0.93–7.52	0.63	0.61	3.77	3.53
SMI	1.29 (0.60)	1.38 (0.41)	1.97 (0.39)	1.89 (0.47)	−0.34–2.14	0.36–2.03	1.21–2.69	0.66–2.98	1.48	1.41	2.00	1.94
FD	2.20 (0.14)	2.21 (0.11)	1.97 (0.19)	2.01 (0.22)	1.83–2.46	1.97–2.46	1.54–2.28	1.52–2.23	2.18	2.21	2.01	2.06
Po (tot) (%)	55.41 (11.47)	56.12 (10.11)	71.27 (11.45)	75.51 (13.35)	28.37–84.63	37.68–75.33	47.42–91.86	53.95–95.23	56.35	55.51	69.00	75.89
Conn.dn ($1/mm^3$)	6.12 (2.63)	6.16 (3.02)	5.79 (3.58)	2.40 (2.04)	1.96–12.28	1.43–12.80	0.30–15.00	0.18–7.40	6.24	6.49	5.53	1.81

TABLE 4 Comparison of Three-Dimensional CBCT Morphometric Parameters for Different Implant Protocols

Morphometric Parameters	Unit	All Regions			
		Control ($n = 9$)	DIP + DL ($n = 10$)	DIP + IL ($n = 9$)	IIP + IL ($n = 8$)
BV/TV	(%)	36.67 ± 13.46	35.28 ± 14.26	37.83 ± 14.62	39.16 ± 15.12
BS/BV	(mm^2/mm^3)	9.52 ± 1.70	13.41 ± 4.13*	12.29 ± 2.82*	12.02 ± 2.27*
Tb.Th	(mm)	0.46 ± 0.07	0.39 ± 0.08*	0.42 ± 0.07	0.41 ± 0.07
Tb.Sp	(mm)	0.79 ± 0.19	0.58 ± 0.12*	0.59 ± 0.15*	0.57 ± 0.17*
Tb.N	(1/mm)	0.80 ± 0.24	0.87 ± 0.24	0.88 ± 0.28	0.92 ± 0.29
Tb.Pf	(1/mm)	1.24 ± 2.17	2.35 ± 2.13	1.45 ± 2.21	1.93 ± 2.48
SMI		1.48 ± 0.74	1.70 ± 0.39	1.54 ± 0.49	1.60 ± 0.55
FD		2.23 ± 0.18	2.04 ± 0.19*	2.10 ± 0.15*	2.08 ± 0.20*
Po (tot)	(%)	63.33 ± 13.46	64.72 ± 14.26	62.17 ± 14.62	60.84 ± 15.13
Conn.dn	($1/mm^3$)	2.47 ± 1.05	6.45 ± 2.79*	6.55 ± 2.41*	6.73 ± 3.66*

Values are shown as mean ± SD.
*Significant difference ($p < 0.001$) between control and treatment groups.

lowest values for Tb.Sp and Po (tot), were found in the IIP + IL group.

DISCUSSION

To our knowledge, this is the first study that uses CBCT imaging to quantitatively examine the effects of different implant protocols on the three-dimensional microstructure of peri-implant bone during a 2-month follow-up, laying the groundwork for clinical application of CBCT imaging for the diagnosis and prognosis of osseointegration. The potential advantages of using CBCT images are the abilities to image noninvasively, to visualize all serial slices for unbiased comparison, and to repeat follow-up measurements, which is almost impossible with histology, where only a limited number of two-dimensional thin slices can be inspected. While it is generally acknowledged that grayscale values in the reconstructed CBCT images do not allow direct assessment of bone mineral density,[18,19] it is feasible to quantify bone structural variables from CBCT images, provided that the spatial resolution is higher than the thinnest trabecular structures.[20] The CBCT imager used in this study can display bone details at a minimum voxel size of 80 µm, which is still finer than the thinnest trabecular thickness of mandibular bone, in both humans and dogs, as revealed by µCT.[21,22] A morphometric analysis of mandibular trabeculae reported that BV/TV obtained using CBCT images was highly correlated with CT values obtained using multislice CT images, suggesting that trabecular morphometry can even be used to evaluate the density of mandibular cancellous bone.[23] In addition to the application reported in human condyle bone,[24] the high-resolution CBCT imager in our study further showed the ability to visualize and analyze peri-implant bone structures in three dimensions.

The present study revealed structural variation of trabecular bone between different anatomical regions, suggesting that coronal and middle bone sections had an optimal trabecular structure around the implant to initiate better modeling or osteogenic responses, while the apical bone section required more bone healing. The coronal and middle regions had higher BV/TV values, indicating a more compact trabecular structure, which corresponds with a lower porosity percentage of bone matrices in this area. This can also be explained by observed thicker trabeculae (higher Tb.Th) with less complexity (lower BS/BV) and more platelike trabecular bone (lower SMI) in the coronal and middle regions. On the contrary, the apical region showed lower FD and Conn.dn, which implies less trabecular bone connectedness exists in this region. Furthermore, the apical trabecular bone had a loose structure (lower Tb.N), which was also reflected in an increased spacing between trabeculae (higher Tb.Sp). The finding is in full accordance with previous studies performed with µCT[25,26] and thus provides the first evidence for CBCT as a reliable modality to analyze trabecular bone.

In view of the paucity of randomized controlled trials applied to compare effects of different implant protocols, we compared all the main available options for implant protocols in both jaws of dogs, ranging from

IIP + IL to DIP + DL, including DIP + IL as well as a natural healing group. The results confirmed significant differences in microstructure parameters between implant protocols and control group, but failed to support the clear superiority of one treatment over the others to achieve remodeling and adaptation of microarchitecture over a 2-month follow-up period. It seems that the mastication, whether biting or chewing forces, received from these implant protocols had some level of significance with controls but was not sensitive enough to have a measurable effect in the microstructures between implant protocols. Moreover, the relatively short observation period of the present examination might be a restriction to a generalization of our findings to humans. It is still unclear to what extent mastication as a separate loading factor can influence the bone microarchitecture and whether it is dominant in initiating the bone remodeling. However, given that the loading protocols may have other confounding factors, such as the strain magnitude and frequency, orientation, and duration of loading,[27–29] the present results probably can be used to establish a lower bound on the achievable accuracy of prediction of morphometric measures by CBCT.

Our results are consistent with those found in other histomorphometric studies on two-dimensional histological slices. Romanos and colleagues[30] reported that in a circle of 500 μm around the implant, no difference existed for BV/TV between DIP + IL and IIP + IL protocols. Later, other researchers indicated that within 2 mm of the implants, loading time does not seem to significantly affect the degree of osseointegration or of BIC or the composition of newly formed bone around dental implants.[31] However, it has also been described in other studies that BV/TV, Tb.Th, and the platelike structure increased according to loadings, mechanical stimulations, or masticatory forces.[26,32,33] Interestingly, though the differences in the parameters between these two protocols were not statistically significant, there was a trend that the IIP + IL group, compared with the DIP + DL group, had more plate-shaped trabeculae (lower SMI and Tb.Pf), denser bone (higher BV/TV), more trabeculae (higher Tb.N), thicker trabeculae (higher Tb.Th), higher trabecular connectivity (lower Po (tot)), and higher structure strength (higher Conn.dn).

However, it should be pointed out that the ROIs were set as far as 1 mm away from the surface of the implant. Generally, the ROIs in the histological analysis of peri-implant bone reactions range from 100 to 300 μm.[34] The adaptive remodeling occurred more frequently nearer to the implant surface in comparison with the areas that are 500 μm away from the implant.[30] Nevertheless, it has also been suggested that the bone remodeling area could extend beyond 500 μm from the implant socket margin.[35] According to a histomorphometric comparison in four species including humans, the remodeling is greatest in the bone adjacent to the interface (i.e., within 1 mm of the implant) and decreases dramatically with increasing distance from the implant.[36] Moreover, a recent study stated that the loading effect seems to decrease along with the distance from the implant, although significant loading effects were found in a distance range of 0 to 1 mm.[37] Of the young generated bone and old degenerated bone around implants, the bone that lies further from the implant (mature bone) has a denser trabecular bone structure, while the bone closer to the implant (younger bone) is more loosely structured, after 2 months of healing.[38] Therefore, over- or underestimations of morphometric parameters may occur depending on how much mature bone is included in the ROIs.

In our study, the voxel size of 80 μm combined with certain exposure situations from the CBCT imager, especially when an initial optimized reconstruction was applied, displayed a high level of bone structural details at the peri-implant level. Yet titanium scatter during CBCT imaging cannot be completely avoided, even when reconstruction algorithms on the imaging data largely compensate for it. This, theoretically, may lead to a deviation between the morphometric parameters obtained from CBCT and histomorphometry, especially at ROIs which are immediately close to the implant. According to μCT findings, a blurred border of 60 μm was found around 3.5 mm-diameter screw-shaped titanium implants.[39] Therefore, a custom-made CTAn protocol was performed in order to automatically exclude implants, and threshold values were chosen manually based on the histogram of each image to correct for metal artifacts. By using this method and adjusting the binary pixels with the histogram, the exact contour of the trabeculae in each image was determined. A drawback of this method is that adjustments are defined visually, resulting in a relative variability of intra- and interobserver measurements. More research is needed to fully standardize imaging processing, minimize artifacts, and optimize reconstruction algorithm and exposure

factors, such as selecting the appropriate FOV or mAs, for potential clinical applications of CBCT in bone structural analyses.

CONCLUSIONS

Despite the limitations, the immediate implant placement and loading protocol may have an improved bone structural integration compared to that obtained by normal extraction healing. The present findings do not seem to suggest a different bone remodeling pattern when a delayed versus an immediate implant placement and loading protocol are used. Additionally, CBCT combined with image processing is a potentially feasible tool in evaluating the complex microarchitecture of peri-implant trabecular bone, opening gates for clinical follow-up analysis of bone healing, whether or not this is peri-implant, and for clinical quality assessment studies.

ACKNOWLEDGMENTS

The authors thank Ms. Zhu Liying, Mr. Zheng Hui, Mr. Li Jiyin, Mr. Yang Ying, and Mr. Na Rishu (Dalian Medical University, China) for their help in the animal experiment. This study was financially supported by grants from the National Natural Science Foundation of China (81000459) and the Chinese Scholarship Council (CSC).

REFERENCES

1. Esposito M, Grusovin MG, Polyzos IP, Felice P, Worthington HV. Interventions for replacing missing teeth: dental implants in fresh extraction sockets (immediate, immediate-delayed and delayed implants). Cochrane Database Syst Rev 2010; (9)CD005968.
2. Schropp L, Isidor F. Timing of implant placement relative to tooth extraction. J Oral Rehabil 2008; 35(Suppl 1):33–43.
3. Kacer CM, Dyer JD, Kraut RA. Immediate loading of dental implants in the anterior and posterior mandible: a retrospective study of 120 cases. J Oral Maxillofac Surg 2010; 68: 2861–2867.
4. Romanos GE, Testori T, Degidi M, Piattelli A. Histologic and histomorphometric findings from retrieved, immediately occlusally loaded implants in humans. J Periodontol 2005; 76:1823–1832.
5. Schincaglia GP, Marzola R, Giovanni GF, Chiara CS, Scotti R. Replacement of mandibular molars with single-unit restorations supported by wide-body implants: immediate versus delayed loading. A randomized controlled study. Int J Oral Maxillofac Implants 2008; 23:474–480.
6. Romanos G, Froum S, Hery C, Cho SC, Tarnow D. Survival rate of immediately vs delayed loaded implants: analysis of the current literature. J Oral Implantol 2010; 36:315–324.
7. Herrmann I, Lekholm U, Holm S, Kultje C. Evaluation of patient and implant characteristics as potential prognostic factors for oral implant failures. Int J Oral Maxillofac Implants 2005; 20:220–230.
8. Griffith JF, Genant HK. Bone mass and architecture determination: state of the art. Best Pract Res Clin Endocrinol Metab 2008; 22:737–764.
9. Müller R, Van Campenhout H, Van Damme B, et al. Morphometric analysis of human bone biopsies: a quantitative structural comparison of histological sections and micro-computed tomography. Bone 1998; 23:59–66.
10. Gomes de Oliveira RC, Leles CR, Lindh C, Ribeiro-Rotta RF. Bone tissue microarchitectural characteristics at dental implant sites. Part 1: identification of clinical-related parameters. Clin Oral Implants Res 2012; 23:981–986.
11. Ladinsky GA, Vasilic B, Popescu AM, et al. Trabecular structure quantified with the MRI-based virtual bone biopsy in postmenopausal women contributes to vertebral deformity burden independent of areal vertebral BMD. J Bone Miner Res 2008; 23:64–74.
12. Issever AS, Link TM, Kentenich M, et al. Assessment of trabecular bone structure using MDCT: comparison of 64- and 320-slice CT using HR-pQCT as the reference standard. Eur Radiol 2010; 20:458–468.
13. Majumdar S. Magnetic resonance imaging for osteoporosis. Skeletal Radiol 2008; 37:95–97.
14. Burghardt AJ, Link TM, Majumdar S. High-resolution computed tomography for clinical imaging of bone microarchitecture. Clin Orthop Relat Res 2011; 469:2179–2193.
15. Vandenberghe B, Jacobs R, Bosmans H. Modern dental imaging: a review of the current technology and clinical applications in dental practice. Eur Radiol 2010; 20:2637–2655.
16. Bouxsein ML, Boyd SK, Christiansen BA, Guldberg RE, Jepsen KJ, Müller R. Guidelines for assessment of bone microstructure in rodents using micro-computed tomography. J Bone Miner Res 2010; 25:1468–1486.
17. Parfitt AM, Drezner MK, Glorieux FH, et al. Bone histomorphometry: standardization of nomenclature, symbols, and units. Report of the ASBMR Histomorphometry Nomenclature Committee. J Bone Miner Res 1987; 2:595–610.
18. Katsumata A, Hirukawa A, Noujeim M, et al. Image artifact in dental cone-beam CT. Oral Surg Oral Med Oral Pathol Oral Radiol Endod 2006; 101:652–657.
19. Pauwels R, Stamatakis H, Manousaridis G, et al. Development and applicability of a quality control phantom for dental cone-beam CT. J Appl Clin Med Phys 2011; 12:245–260.
20. Kothari M, Keaveny TM, Lin JC, Newitt DC, Genant HK, Majumdar S. Impact of spatial resolution on the prediction of trabecular architecture parameters. Bone 1998; 22:437–443.

21. Giesen EB, van Eijden TM. The three-dimensional cancellous bone architecture of the human mandibular condyle. J Dent Res 2000; 79:957–963.
22. Imoto H, Yamada A, Shimamura I, Matsunaga S, Ide Y. Influence of mechanical loading on resonance frequency analysis and trabecular structure of peri-implant bone. Prosthodont Res Pract 2007; 6:120–126.
23. Naitoh M, Aimiya H, Hirukawa A, Ariji E. Morphometric analysis of mandibular trabecular bone using cone beam computed tomography: an in vitro study. Int J Oral Maxillofac Implants 2010; 25:1093–1098.
24. Liu SM, Zhang ZY, Li JP, Liu DG, Ma XC. [A study of trabecular bone structure in the mandibular condyle of healthy young people by cone beam computed tomography]. Zhonghua Kou Qiang Yi Xue Za Zhi 2007; 42:357–360.
25. van Ruijven LJ, Giesen EB, Mulder L, Farella M, van Eijden TM. The effect of bone loss on rod-like and plate-like trabeculae in the cancellous bone of the mandibular condyle. Bone 2005; 36:1078–1085.
26. Moon HS, Won YY, Kim KD, et al. The three-dimensional microstructure of the trabecular bone in the mandible. Surg Radiol Anat 2004; 26:466–473.
27. Grunheid T, Langenbach GE, Brugman P, Everts V, Zentner A. The masticatory system under varying functional load. Part 2: effect of reduced masticatory load on the degree and distribution of mineralization in the rabbit mandible. Eur J Orthod 2011; 33:365–371.
28. Zhang X, Vandamme K, Torcasio A, et al. In vivo assessment of the effect of controlled high- and low-frequency mechanical loading on peri-implant bone healing. J R Soc Interface 2012; 9:1697–1704.
29. Barak MM, Lieberman DE, Hublin JJ. A Wolff in sheep's clothing: trabecular bone adaptation in response to changes in joint loading orientation. Bone 2011; 49:1141–1151.
30. Romanos GE, Toh CG, Siar CH, Wicht H, Yacoob H, Nentwig GH. Bone-implant interface around titanium implants under different loading conditions: a histomorphometrical analysis in the *Macaca fascicularis* monkey. J Periodontol 2003; 74:1483–1490.
31. Ghanavati F, Shayegh SS, Rahimi H, Sharifi D, Khalesseh N, Eslami B. The effects of loading time on osseointegration and new bone formation around dental implants: a histologic and histomorphometric study in dogs. J Periodontol 2006; 77:1701–1707.
32. Borah B, Dufresne TE, Cockman MD, et al. Evaluation of changes in trabecular bone architecture and mechanical properties of minipig vertebrae by three-dimensional magnetic resonance microimaging and finite element modeling. J Bone Miner Res 2000; 15:1786–1797.
33. Rubin C, Turner AS, Müller R, et al. Quantity and quality of trabecular bone in the femur are enhanced by a strongly anabolic, noninvasive mechanical intervention. J Bone Miner Res 2002; 17:349–357.
34. Corpas Ldos S, Jacobs R, Quirynen M, Huang Y, Naert I, Duyck J. Peri-implant bone tissue assessment by comparing the outcome of intra-oral radiograph and cone beam computed tomography analyses to the histological standard. Clin Oral Implants Res 2011; 22:492–499.
35. Futami T, Fujii N, Ohnishi H, et al. Tissue response to titanium implants in the rat maxilla: ultrastructural and histochemical observations of the bone-titanium interface. J Periodontol 2000; 71:287–298.
36. Garetto LP, Chen J, Parr JA, Roberts WE. Remodeling dynamics of bone supporting rigidly fixed titanium implants: a histomorphometric comparison in four species including humans. Implant Dent 1995; 4:235–243.
37. Ogawa T, Zhang X, Naert I, et al. The effect of whole-body vibration on peri-implant bone healing in rats. Clin Oral Implants Res 2011; 22:302–307.
38. Cochran DL. The evidence for immediate loading of implants. J Evid Based Dent Pract 2006; 6:155–163.
39. Stoppie N, van der Waerden JP, Jansen JA, Duyck J, Wevers M, Naert IE. Validation of microfocus computed tomography in the evaluation of bone implant specimens. Clin Implant Dent Relat Res 2005; 7:87–94.